J. Fluid Mech. (1989), *vol.* 203, *pp.* 125–148
Printed in Great Britain

Flow in curved ducts: bifurcation structure for stationary ducts

By P. DASKOPOULOS AND A. M. LENHOFF
Department of Chemical Engineering, University of Delaware, Newark, DE 19716, USA

(Received 12 August 1987 and in revised form 11 July 1988)

In developed laminar flow in stationary curved ducts there is, in addition to the two-vortex secondary flow structure first analysed by Dean (1927), another solution branch with a four-vortex secondary flow. These two branches have recently been shown to be joined by a third branch, but stability characteristics and the possible presence of additional branches have yet to be described. In this paper orthogonal collocation is used in conjunction with continuation techniques to characterize the bifurcation structure for symmetric flows. The two- and four-vortex solutions are stable to symmetric disturbances, while the recently reported branch joining them is unstable. A more systematic exploration of the parameter space than has hitherto been reported is performed by examining the morphogenesis of the bifurcation structure within the general framework of properties described by Benjamin (1978). The starting point is the 'perfect' problem of flow in an infinite curved slit, which bifurcates to give rise to a cellular structure. Addition of 'stickiness' at the cell boundaries turns each pair of cells into a curved duct of rectangular cross-section which, by a geometry change, leads to the curved circular tube. For the perfect problem a large number of solution branches are present, but the addition of stickiness turns most of them into isolae which vanish before the no-slip limit is reached. The solution branches that remain include, in addition to the three described previously, another solution family not connected to the other one. This family comprises two branches, both four-vortex in character and unstable to symmetric disturbances.

1. Introduction

The pressure-driven laminar flow of an incompressible Newtonian fluid in a curved tube of circular cross-section was first considered by Dean (1927, 1928*a*). Since then, a substantial body of experimental, theoretical and numerical work has accumulated dealing with the problem of viscous flow in curved ducts of various cross-sections; the flows in all of them are qualitatively similar at low flow rates, with Dean's results providing a good picture. Laminar flow through the tube is accompanied by the development of a secondary flow consisting of a pair of counter-rotating vortices, giving rise to helical streamlines. The secondary flow is caused by the action of the centrifugal force driving the fluid towards the outer wall of the pipe, near which it is slowed down by viscous forces. The fluid pushed to the outer wall then moves inward along the walls until it reaches the inner bend, from where it repeats its cyclic motion.

The detailed character of the flow can be significantly more complex than that described by Dean, even in the limit of small curvature for which his development is valid. The system is characterized by a single dimensionless parameter, today

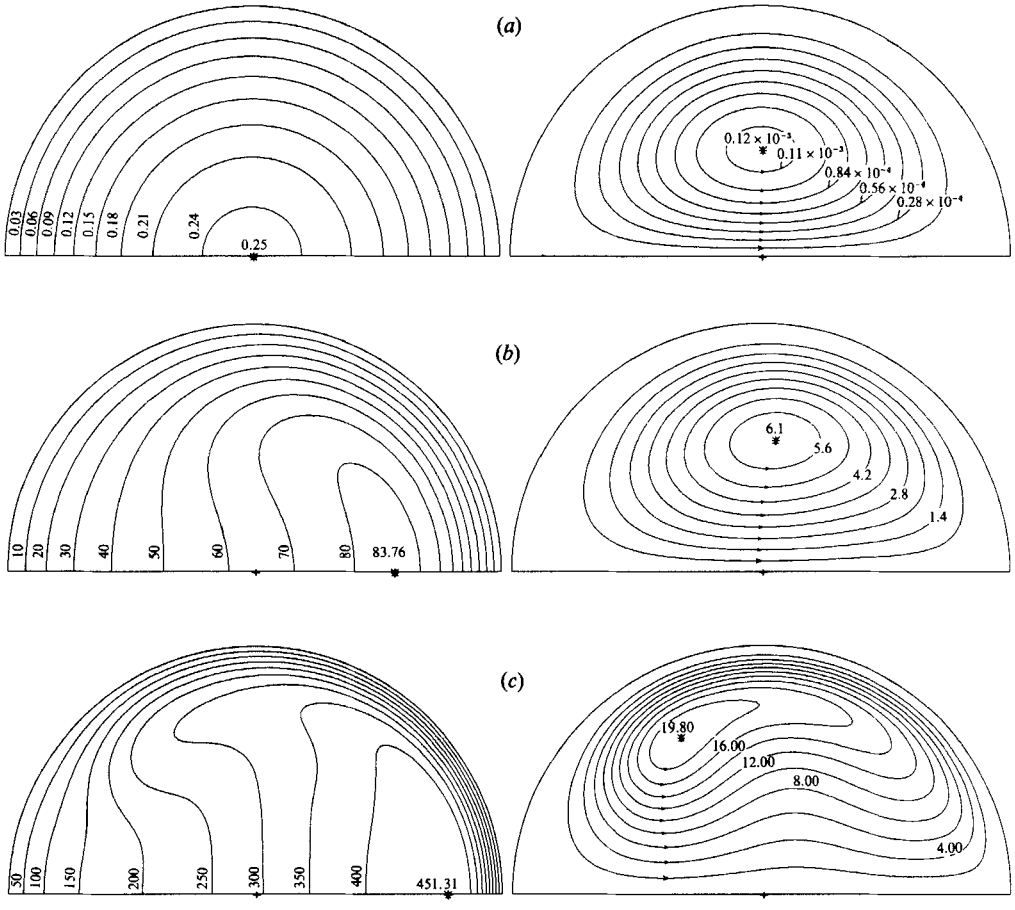

FIGURE 1. Axial velocity contours and two-vortex secondary flow streamlines. (*a*) $D = 1$; (*b*) 500; (*c*) 5000.

known as the Dean number D. A number of variants exist (Van Dyke 1978; Berger, Talbot & Yao 1983), but all vary as $\delta^{\frac{1}{2}}Re$, with δ the curvature and Re the Reynolds number. The Dean number provides a measure of the importance of inertial and centrifugal forces relative to viscous forces, and since secondary flows result from the interaction of centrifugal and viscous forces, the Dean number provides an estimate of their strength. This effect may be seen in figure 1, which shows axial velocity contours and secondary flow streamlines computed by the procedure discussed in §3; these results are in excellent agreement with those reported previously (e.g., Dean 1927, 1928*a*; McConalogue & Srivastava 1968; Collins & Dennis 1975; and many other contributors, with a comprehensive review presented by Berger *et al.* 1983, and more recently by Itō 1987). For small values of D the flow field is roughly symmetric about a line through the centre of the duct parallel to the axis about which the tube is coiled (figure 1*a*). As D is increased the axial velocity contours and the secondary flow streamlines tend to become distorted and the locations of the maximum in axial velocity and of the centre of the secondary flow vortex move towards the outer wall (figure 1*b*). At even larger values of D, the vortex centre moves back toward the inner wall of the tube (figure 1*c*), with boundary layers developing near the walls of the pipe while the core appears to be inviscid (Barua 1963).

Flow in curved ducts of other cross-sections have similar characteristics, but an additional feature is the existence of a four-vortex solution reported for rectangular ducts (Cheng & Akiyama 1970; Joseph, Smith & Adler 1975; De Vriend 1981; Winters & Brindley 1984; Shanthini & Nandakumar 1986; Winters 1987; Soh 1988) and for semicircular ducts (Masliyah 1980; Nandakumar & Masliyah 1982). A four-vortex flow has also been observed experimentally by flow visualization in rectangular ducts by Cheng, Nakayama & Akiyama (1979) and in semicircular ducts by Masliyah (1980). This feature was subsequently described for circular ducts by Dennis & Ng (1982) and Nandakumar & Masliyah (1982) for values of $D > 956$; Cheng, Inaba & Akiyama (1985) verified the numerical predictions experimentally by flow visualization. These studies did not, however, resolve the issue of how the two- and four-vortex flows are related, although Nandakumar, Masliyah & Law (1985), in a paper dealing with bifurcation in steady laminar mixed convection flow in horizontal ducts, pointed out the similarities with the problem of flow in curved pipes, and suggested that instead of one critical Dean number, there should be a lower and an upper critical value of the flow parameter. This would define a region of coexistence of the two solutions, with only a four-vortex flow pattern existing above the upper critical value and only the two-vortex one below the lower critical value.

The objectives of the present work were to elucidate the relationship between the two solution branches, and to obtain a more complete picture of bifurcation phenomena, including the possible existence of additional solutions and the stability of solutions. Although these goals were indeed accomplished, we became aware after submitting this paper for review that several important features of the relationship had already been reported. Winters & Brindley (1984), in a preliminary report dealing mainly with ducts of rectangular cross-section, identified a solution branch linking the two- and four-vortex branches, as suggested (subsequently) by Nandakumar *et al.* (1985). An expanded treatment of the bifurcation structure, but only for ducts of rectangular cross-section, was presented by Winters (1987). For circular ducts, Yang & Keller (1986*a*, *b*) verified the existence of multiple solutions and, in fact, reported four folds and hence five solution branches. Their conjecture was that the problem has an infinite number of possible solutions, exhibiting $2n$-vortex character. Furthermore, they stressed the need for more accurate calculation in order to elucidate the rule of formation of new solution branches. They did not determine the stability characteristics of their solution branches.

Thus although some of the features of flow in curved ducts we set out to characterize had been described previously, several issues remain unresolved. This paper addresses these issues using a computational approach in which multiple solution branches may be expected to be located more systematically than in previous studies of flow in curved ducts.

2. Outline of approach

A more complete characterization of flow in curved ducts requires a systematic approach for exploring the parameter space. For this we make use of the work of Benjamin (1978), whose discussion deals both with the generic properties of flow bifurcations and with morphogenesis of flow patterns as flow or geometric parameters change. The results apply to solutions of the Navier–Stokes equations in a finite domain.

Benjamin treats the generic properties by assuming that, for any given geometry,

the flow is characterized by a single parameter; he uses the Reynolds number, but for flow in a curved duct of small curvature the Dean number serves the same purpose. The Navier–Stokes equations then have, for all finite D, at least one solution. For sufficiently small D there is a unique, unconditionally stable (primary) solution, while bifurcations may occur at higher D. When they do, the solutions to the steady-state problem are isolated and odd in number (except at discrete critical values of D where bifurcations occur); for k possible flows, at least $\frac{1}{2}(k-1)$ of them are unstable. For any physically attainable flows, supercritical and subcritical bifurcations are impossible. As Benjamin states, these bifurcations 'belong rather to idealized theoretical models whose perfect symmetry allows the exceptional behaviour, and ... they are changed into smooth processes under the influence of the imperfections always present in practice'. For real systems, he states that if two-sided bifurcations occur, they will be transcritical, although one-sided bifurcations are likely to predominate.

These principles can be applied to the known characteristics of flow in curved ducts. The two-vortex solution is the primary solution, while the four-vortex solution appears at a bifurcation point which, for ducts of circular cross-section, appears to be at around $D = 956$. The stability of these solutions has been examined only superficially for circular ducts (Winters & Brindley 1984), and even these results may be unreliable because of the possible existence of spurious eigenvalues. However, both branches may be assumed to be stable: the primary (two-vortex) solution is known to be unconditionally stable, while the fact that convergence to the four-vortex solution has been observed both computationally and experimentally suggests that it, too, is stable. From the properties listed by Benjamin and summarized above it can be concluded that there is at least one additional solution, that it is unstable, and that at a bifurcation point at about $D = 956$ this solution joins up with the four-vortex solution; Winters & Brindley (1984) and Yang & Keller (1986*a*, *b*) found this solution computationally.

The picture is not yet necessarily complete, however, at least in part because the generic properties deal with transitions as D is increased from small values, where there is a unique solution; they are not particularly informative regarding bifurcation phenomena at higher D. For instance, whether the bifurcation described is transcritical or one-sided depends on what happens at higher D. In addition, there may be other one-sided bifurcations from which arise branches not yet known to exist. In order to fill in at least some of the blanks, we can use Benjamin's second parameter, that describing system boundaries, and use as a starting point a 'perfect' system for which supercritical and subcritical bifurcations are possible. Then, by changing the system boundaries and the conditions applying there, we can continuously add the imperfections that ultimately transform the perfect system into the imperfect (physically realizable) one in which we are interested.

Nandakumar & Masliyah (1982) used this result in going from the known four-vortex solution in a semicircular duct to that in a circular one; they thus went from one imperfect situation to another. We use it in a different way, starting from the perfect problem of developed laminar flow in a curved slit of infinite extent along the axis of curvature. The low-D flow here is then just slit Poiseuille flow. At some critical D, a bifurcation occurs, giving rise to a periodic structure similar to that in Couette flow, associated with Taylor (1923). As Benjamin explains, two periodic structures in an infinite domain differing only by a half-period shift must have identical properties; consequently, the bifurcation diagram must, at least at the bifurcation point, be symmetric about the primary solution, i.e. supercritical or subcritical.

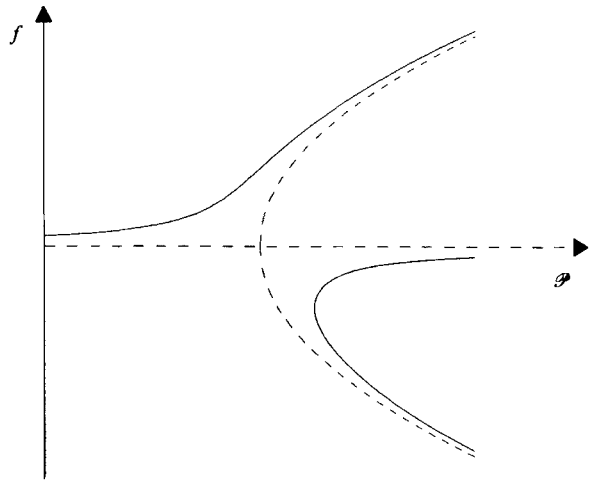

FIGURE 2. Effect on bifurcation structure of deviation from 'perfect' problem. Broken line represents perfect problem, solid line real problem. (After Benjamin 1978).

Because the choice of state variables is arbitrary, this symmetry does not necessarily persist beyond the bifurcation point. More important is that the symmetry is broken by adding an imperfection to the problem in the form of some 'stickiness' along the cell boundary; the result is qualitatively similar to that illustrated in figure 2 for Benjamin's algebraic example. Note, however, that the resulting bifurcation diagram still resembles that for the perfect problem.

Steady addition of stickiness corresponds to going in continuous fashion from the perfect problem to the corresponding situation with no slip at cell boundaries, the bifurcation diagram thus going systematically to that for flow in a curved duct of rectangular cross-section. A change in geometry then allows the duct of circular cross-section to be obtained. The implementation of this procedure will be described in the following sections.

3. Problem formulation and solution

3.1. *Describing equations*

While the procedure described above forms the framework within which flow characteristics will be established, the actual solutions on different branches of the bifurcation diagram must still be found by solving the Navier–Stokes equations for the respective systems considered. The equations and solution methods will be discussed here for curved ducts of circular cross-section; other geometries were treated similarly, and will be discussed briefly as they arise.

For ducts of circular cross-section, an orthogonal toroidal system of coordinates will be used, as shown in figure 3. The system of coordinates is identical to that used by most previous investigators, such as Dennis & Ng (1982) and McConalogue & Srivastava (1968), and differs from the original one proposed by Dean (1927, 1928*a*) only in the direction of the azimuthal angle. OZ represents the axis around which the tube is coiled, C denotes the tube centre, $OC = R$ is the radius of curvature of the tube and a its radius. The axial distance is expressed in terms of an angle θ measured from a fixed axial plane and increasing along the direction of the primary flow. The centre of the coordinate system is fixed at the tube centre, with the coordinates of any point

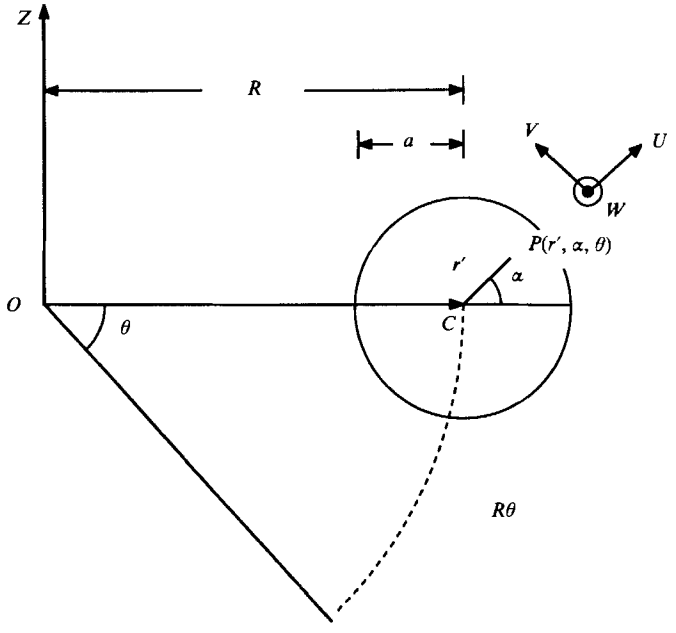

FIGURE 3. Toroidal coordinate system.

P denoted by (r', α, θ) and corresponding velocity components by (U, V, W). The flow is caused by a constant axial pressure gradient $G = -R^{-1}(\partial p/\partial\theta)$. Steady, fully developed flow is considered, so that the velocity components are independent of θ and of time; the primary (axial) flow is locally rectilinear and the study of the secondary flow can be limited to the two-dimensional cross-section.

Dimensionless variables are introduced by scaling relative to quantities that render the centrifugal terms, driving the secondary flow, of the same order of magnitude as viscous and inertial effects:

$$r = \frac{r'}{a}, \quad u = \frac{aU}{\nu}, \quad v = \frac{aV}{\nu}, \quad w = \frac{aW}{\nu}\left(\frac{2a}{R}\right)^{\frac{1}{2}}, \tag{1}$$

where ν is the kinematic viscosity. A stream function $\psi(r, \alpha)$ identically satisfies the continuity equation in the limit of negligible curvature, $\delta = (a/R) \to 0$, with

$$u = \frac{1}{r}\frac{\partial\psi}{\partial\alpha}, \quad v = -\frac{\partial\psi}{\partial r}. \tag{2}$$

The Navier–Stokes equations in the limit of negligible curvature were originally derived by Dean (1927):

$$\nabla^2 w + \frac{1}{r}\left(\frac{\partial\psi}{\partial r}\frac{\partial w}{\partial a} - \frac{\partial\psi}{\partial\alpha}\frac{\partial w}{\partial r}\right) = -D, \tag{3}$$

$$\nabla^4\psi + \frac{1}{r}\left(\frac{\partial\psi}{\partial r}\frac{\partial}{\partial\alpha} - \frac{\partial\psi}{\partial\alpha}\frac{\partial}{\partial r}\right)\nabla^2\psi = -w\left(\sin\alpha\frac{\partial w}{\partial r} + \frac{\cos\alpha}{r}\frac{\partial w}{\partial\alpha}\right), \tag{4}$$

where

$$\nabla^2 = \frac{\partial^2}{\partial r^2} + \frac{1}{r}\frac{\partial}{\partial r} + \frac{1}{r^2}\frac{\partial^2}{\partial\alpha^2}, \tag{5}$$

$$\nabla^4 = \nabla^2\nabla^2, \tag{6}$$

and D is the Dean number defined as

$$D = \frac{Ga^3}{\mu\nu}\left(\frac{2a}{R}\right)^{\frac{1}{2}} \tag{7}$$

with μ the dynamic viscosity. The particular variant of Dean number used is the one arising naturally from the describing equations and the scaling used. It is equivalent to a Reynolds number multiplied by the square-root of the curvature, with the characteristic axial velocity taken as that for fully developed flow in a straight tube with the same pressure gradient.

Like most previous studies, ours is limited to symmetric solutions; additional solutions may exist if this constraint is relaxed, as shown by Winters (1987) for rectangular ducts. The boundary conditions imposed by the geometry of the system are then no-slip condition at the walls:

$$w = \psi = \frac{\partial\psi}{\partial r} = 0 \quad \text{for} \quad r = 1; \tag{8}$$

symmetry about the central plane of the tube (OC in figure 3) for all velocity components:

$$\frac{\partial w}{\partial\alpha} = \frac{\partial\psi}{\partial r} = \frac{1}{r}\frac{\partial^2\psi}{\partial\alpha^2} = 0 \quad \text{at} \quad \alpha = 0, \pi; \tag{9}$$

stream function along the plane of symmetry:

$$\psi(r, 0) = \psi(r, \pi) = 0; \tag{10}$$

conditions along plane of symmetry applied at tube centre:

$$\frac{\partial w}{\partial r} = \psi = \frac{1}{r}\frac{\partial\psi}{\partial\alpha} = \frac{\partial^2\psi}{\partial r^2} = 0 \quad \text{at} \quad r = 0, \quad \alpha = \tfrac{1}{2}\pi. \tag{11}$$

The symmetry along the central plane also allows the reduction of the computational domain to the upper semicircular region of the tube cross-section $0 \leqslant r \leqslant 1$, $0 \leqslant \alpha \leqslant \pi$.

3.2. *Solution procedure*

Because the system has boundaries described explicitly in terms of coordinate surfaces, global weighted residual methods are suitable for solving the equations; they also have the advantage of providing a continuous function as a solution over the entire computational domain. Orthogonal collocation was the procedure selected. The basis functions used were Fourier series in the azimuthal direction, due to the periodicity of the problem, and Chebyshev polynomials in r, in order to minimize the maximum error of the interpolation (Lanczos 1956). The expansions used were of the form

$$w = (1-r^2)\sum_{i=0}^{N} w_{2i,0}P_{2i}(r) + (1-r^2)\sum_{i=0}^{N}\sum_{j=0}^{M} w_{2i+1,2j+1}P_{2i+1}(r)\cos((2j+1)\alpha) + (1-r^2)r^2\sum_{i=0}^{N}\sum_{j=1}^{M} w_{2i,2j}P_{2i}(r)\cos(2j\alpha), \tag{12}$$

$$\psi = r(1-r^2)^2\sum_{i=0}^{N}\sum_{j=0}^{M} \psi_{2i,2j+1}P_{2i}(r)\sin((2j+1)\alpha) + r(1-r^2)^2\sum_{i=0}^{N}\sum_{j=1}^{M+1} \psi_{2i+1,2j}P_{2i+1}(r)\sin(2j\alpha) \tag{13}$$

in order to satisfy the constraints imposed by the boundary conditions and system symmetry, where $P_k(r)$ are Chebyshev polynomials of order k.

Substitution into the differential equations (3) and (4) and setting the residuals equal to zero at a set of collocation points yields an algebraic system of $4(N+1)(M+1)$ equations, from which the coefficients in the expansions can be found using an iterative or a direct technique. The collocation points were chosen as the roots of the orthogonal function sets used in the trial solution. Thus the points in the azimuthal direction were the roots in $(0, \pi)$ of

$$\cos(2(M+1)\alpha) = 0 \tag{14}$$

and those in the radial direction were the positive roots of

$$P_{2(N+1)}(r) = 0. \tag{15}$$

For a given expansion order the problem is thus reduced to a system of algebraic equations of the form

$$\boldsymbol{R}(\boldsymbol{x}, D) = \boldsymbol{0}, \tag{16}$$

where $\boldsymbol{R}$ are the residuals at the collocation points and $\boldsymbol{x}$ the vector of coefficients to be calculated. Equation (16) was solved using Newton's method with the termination criterion

$$\|\boldsymbol{x}^{(n+1)} - \boldsymbol{x}^{(n)}\|_\infty \leqslant 10^{-12}\|\boldsymbol{x}^{(n)}\|_\infty, \tag{17}$$

where the superscripts denote iteration numbers. Poiseuille flow at low Dean numbers represents a suitable initial guess, and zeroth- and first-order continuation methods were used to advance in the parameter space D. No convergence problems were encountered over the entire range of D considered. Solution branches could be followed easily, except in the neighbourhood of singular points, where the determinant of the Jacobian vanishes. In these cases an arclength continuation technique (Keller 1977, 1982) was used to follow the turning behaviour of the solution branch.

3.3. *Stability*

If the time-dependent terms are retained, the Navier–Stokes equations take the form (cf. (3) and (4))

$$\frac{\partial w}{\partial \tau} = \nabla^2 w + \frac{1}{r}\left(\frac{\partial \psi}{\partial r}\frac{\partial w}{\partial \alpha} - \frac{\partial \psi}{\partial \alpha}\frac{\partial w}{\partial r}\right) + D, \tag{18}$$

$$\frac{\partial}{\partial \tau}(\nabla^2 \psi) = \nabla^4 \psi + \frac{1}{r}\left(\frac{\partial \psi}{\partial r}\frac{\partial}{\partial \alpha} - \frac{\partial \psi}{\partial \alpha}\frac{\partial}{\partial r}\right)\nabla^2 \psi + w\left(\sin\alpha \frac{\partial w}{\partial r} + \frac{\cos\alpha}{r}\frac{\partial w}{\partial \alpha}\right), \tag{19}$$

where time is scaled as $\tau = \nu t/a^2$. After substitution of the expansions used from (12) and (13), the system equations can be written in matrix form as

$$\boldsymbol{A}\frac{\partial \boldsymbol{x}}{\partial \tau} = \boldsymbol{R}(\boldsymbol{x}, D), \tag{20}$$

where $\boldsymbol{A}$ is a constant non-singular premultiplying matrix.

If $\boldsymbol{x}^0$ denotes a steady-state solution and $\boldsymbol{d} = \boldsymbol{x} - \boldsymbol{x}^0$ a small disturbance, (20) becomes, after linearization about the steady state,

$$\frac{\partial \boldsymbol{d}}{\partial \tau} = \frac{\partial \boldsymbol{x}}{\partial \tau} = \boldsymbol{A}^{-1}\frac{\partial \boldsymbol{R}}{\partial \boldsymbol{x}}(\boldsymbol{x}^0, D)\,\boldsymbol{d}. \tag{21}$$

By the first Liapunov method (Kubíček & Marek 1983), the steady-state solution is stable if all eigenvalues of the matrix $\boldsymbol{A}^{-1}(\partial \boldsymbol{R}/\partial \boldsymbol{x})$ have negative real parts. Changes

in sign of eigenvalues can be detected by examining the sign of the determinant, except for complex-conjugate pairs. Some caution is needed, though, because the numerical method used introduces spurious eigenvalues and even multiple singular points (Gottlieb & Orszag 1977). Since the spurious eigenvalues tend to have large growth rates with grid refinement, real and spurious eigenvalues were distinguished by calculating the eigenvalues for expansions of different order. Those eigenvalues that were constant for different orders were classified real and those that changed were considered spurious; the latter typically represented only a small fraction of the total number. It is important to bear in mind that, since the trial functions (12) and (13) satisfy the symmetry conditions (9), (10) and (11), the stability properties obtained apply only to stability to symmetric disturbances. Winters (1987) deals with asymmetric disturbances in ducts of rectangular cross-section.

4. Results and discussion

4.1. *Circular ducts*

Steady-state solutions to (3) and (4) were obtained for values of D throughout the laminar flow regime, and beyond. The criterion used for determining a suitable order of expansion was based on the relative improvement resulting from an increase in order,

$$\frac{\int_0^{\pi}\int_0^1 (\psi^1-\psi^0)^2\, r\,\mathrm{d}r\,\mathrm{d}\alpha}{\int_0^{\pi}\int_0^1 (\psi^0)^2\, r\,\mathrm{d}r\,\mathrm{d}\alpha}, \tag{22}$$

where ψ^1 denotes the $(N+1, M)$ or $(N, M+1)$ order approximation and ψ^0 the (N, M) one. This criterion was found to be more stringent than the corresponding one for the axial velocities and hence was used over the whole range of D-values. A typical requirement for indicating that the expansion was of sufficiently high order was that (22) take a value of the order of 10^{-6}. The required number of collocation points increases with D, as would be expected. An expansion with $N = 10$ and $M = 7$ proved adequate for the parameter space up to $D \sim 5000$ and required 2–3 minutes of CPU time on a DEC VAX 11/785 for each iteration. Three or four iterations were typically needed for the continuation algorithm to satisfy the criterion (17). The rate of convergence was quadratic as expected, except in the neighbourhood of singular points.

For small D, where Dean's results apply, excellent agreement with his perturbation solution was observed for $D < 50$, with deviations apparent only for $D > 70$; the upper limit of validity of the perturbation solution, as determined by Dean (1928*a*), is $D = 96$. The order of the expansion needed for a satisfactory approximation in this region is small ($N = 4$ and $M = 3$), and less than one second of CPU time was required. At higher Dean numbers the results obtained for the two-vortex solution agree with essentially all other reported results, in particular those of McConalogue & Srivastava (1968), Collins & Dennis (1975) and Yang & Keller (1986*a*, *b*). Some velocity contours and streamlines are shown in figure 1, with the values of the contours labelled and the position of the maximum in axial velocity and the vortex centre denoted by an asterisk in the respective diagrams. Our results show the two-vortex solution to exist as a stable solution to the problem for all D in the laminar flow region (up to $D \sim 5000$).

The two-vortex solution is the unique, unconditionally stable solution for Dean

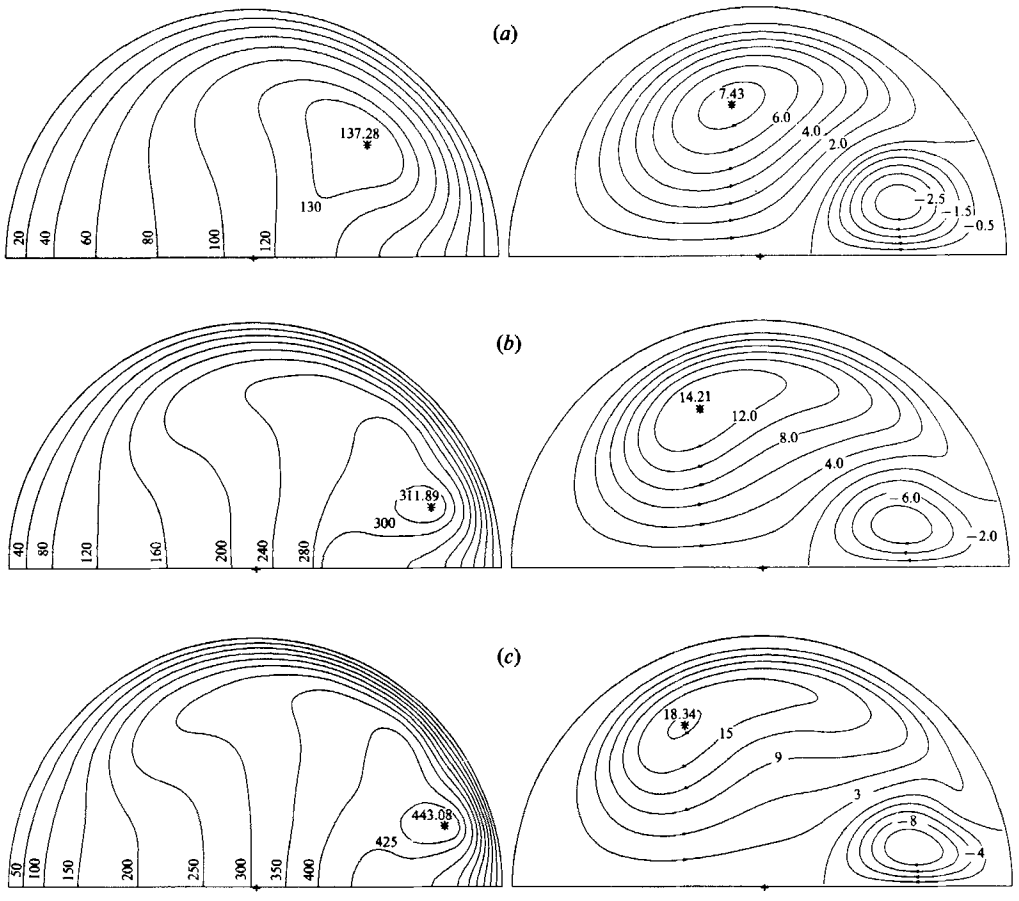

FIGURE 4. Axial velocity contours and secondary flow streamlines for stable four-vortex solution. (*a*) $D = 1000$; (*b*) 3000; (*c*) 5000.

numbers up to approximately $D = 956$, where Dennis & Ng (1982) and Nandakumar & Masliyah (1982) found a four-vortex solution to appear. Being unaware of the direct link between the branches found by Winters & Brindley (1984) and Yang & Keller (1986*a*, *b*), we started our continuation scheme on the four-vortex branch using an initial guess close to the results of Dennis & Ng (1982) for $D = 5000$. The iterative scheme used to solve (16) converged to a stable solution, which was followed down to $D = 955.7259$, where a singular point was detected. Figure 4 shows some representative solutions from that branch; they agree well with those of Dennis & Ng and Nandakumar & Masliyah.

Traversal of the turning point leads to the third solution, which proved to be unstable, as expected from the generic properties described by Benjamin (1978) and discussed in §2. Characteristic axial velocity profiles and streamlines from solutions in this family are shown in figure 5. This solution is also four-vortex in character, but different from the stable one in the nature of the vortex near the outer wall of the tube. In the stable solution the vortex area is approximately constant across the whole parameter space and the vortex becomes stronger as D increases, whereas on the unstable branch the vortex shrinks and weakens as D increases, and the axial velocity profiles are similar to those of the two-vortex family. Thus the unstable

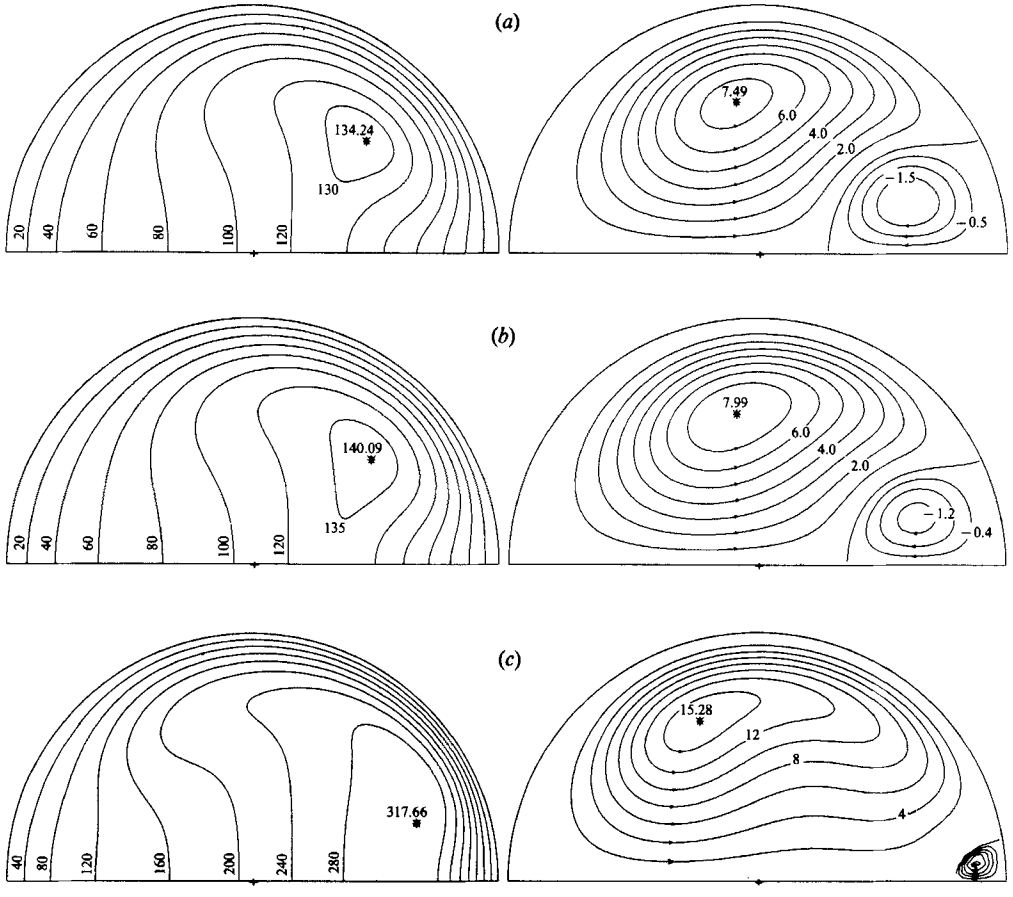

FIGURE 5. Axial velocity contours and secondary flow streamlines for unstable solution. (*a*) $D = 955.9$; (*b*) 1000; (*c*) 3000.

branch seems to be much like the two-vortex solution in character; indeed, Yang & Keller (1986*a*) show only a two-vortex secondary flow on this branch.

Additional refined calculations, performed on a Cray X-MP/48 because of the requirements of a bigger system (an expansion of $N = 19$, $M = 16$ was required for reliable results at large D), examined the parameter space for $D > 5000$ in order to explore the relationships between the different branches. No dramatic qualitative changes in flow behaviour are observed at these very high Dean numbers, but because the analysis is restricted to symmetric disturbances this result is not physically meaningful. It is, however, relevant to the discussion of morphogenesis of the bifurcation diagram, in §4.2. The computations showed the primary two-vortex solution and the unstable branch to meet at a turning point at a D-value which decreased as more refined grids were used, the value for the largest expansion being about 32510. By comparison, Yang & Keller's (1986*a*) turning-point Dean number increased with grid refinement, their most accurate value for loosely coiled tubes being $D = 25146$. It is interesting to note that Soh & Berger (1987) were able to find only the two-vortex solution even for values of D as high as 30000. As regards the stable four-vortex branch, we followed it, too, up to $D \sim 35000$, but saw no indication of further turning points, although Yang & Keller found one at $D = 15642$

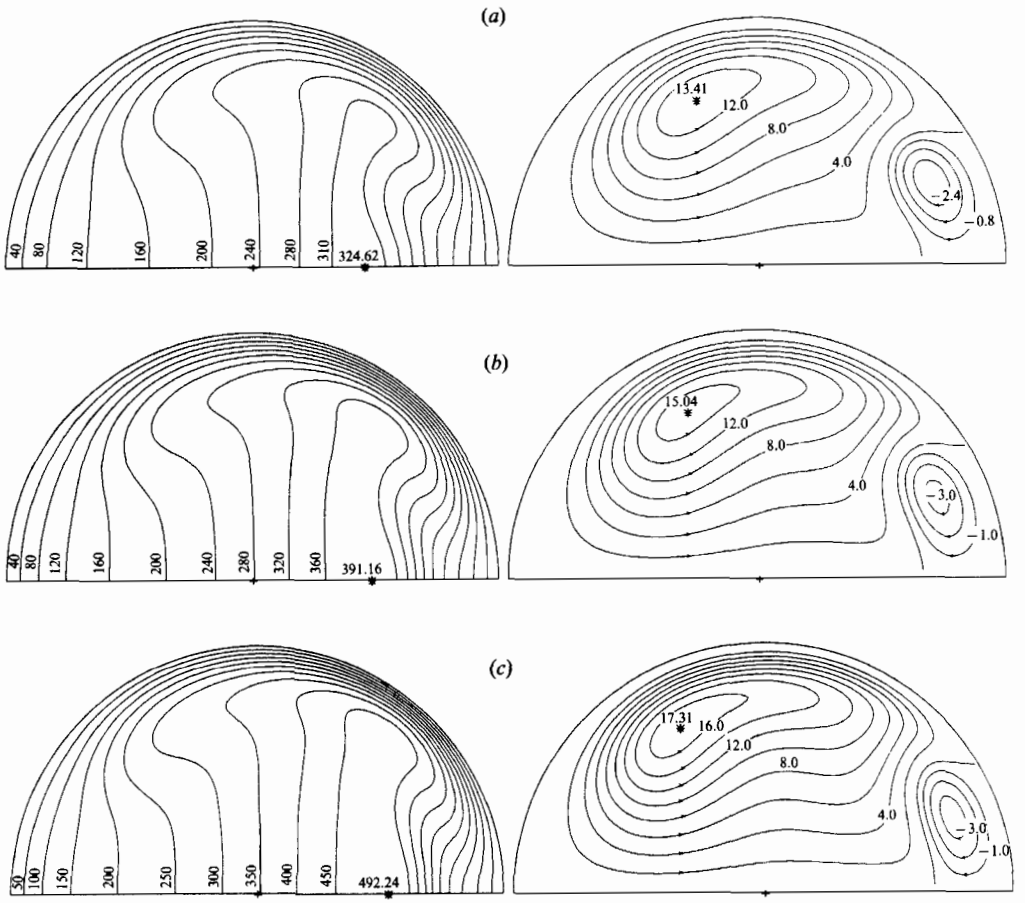

FIGURE 6. Axial velocity contours and secondary flow streamlines for singly unstable branch of second solution family. (*a*) $D = 3100$; (*b*) 4000; (*c*) 5500.

for their most refined calculations. We are unable to explain this difference; the most useful approach to resolution of the discrepancy is probably further grid refinement in their method.

In addition to the solution families described thus far, another solution family has been located via the morphogenesis characterization described in §4.2. This family consists of two branches and appears to be unconnected to the three solutions described previously, at least for values of D up to about 35000. The two branches differ in several respects from Yang & Keller's (1986*a*) fourth and fifth branches, so they almost certainly represent different solutions. Both branches are unstable, with one branch (characterized by two positive eigenvalues) exhibiting four-vortex character, going through a turning point at $D = 2494.218$ and giving rise to another unstable branch (one positive eigenvalue) developing more and more two-vortex character. Characteristic axial velocity profiles and streamlines for the two branches are shown in figures 6 and 7 respectively. To our knowledge this is the first time a solution like this has been reported for curved ducts of circular cross-section, although Winters (1987) reports a qualitatively similar solution for square ducts (see further discussion later).

A property used in the literature for comparing the two stable solutions is the

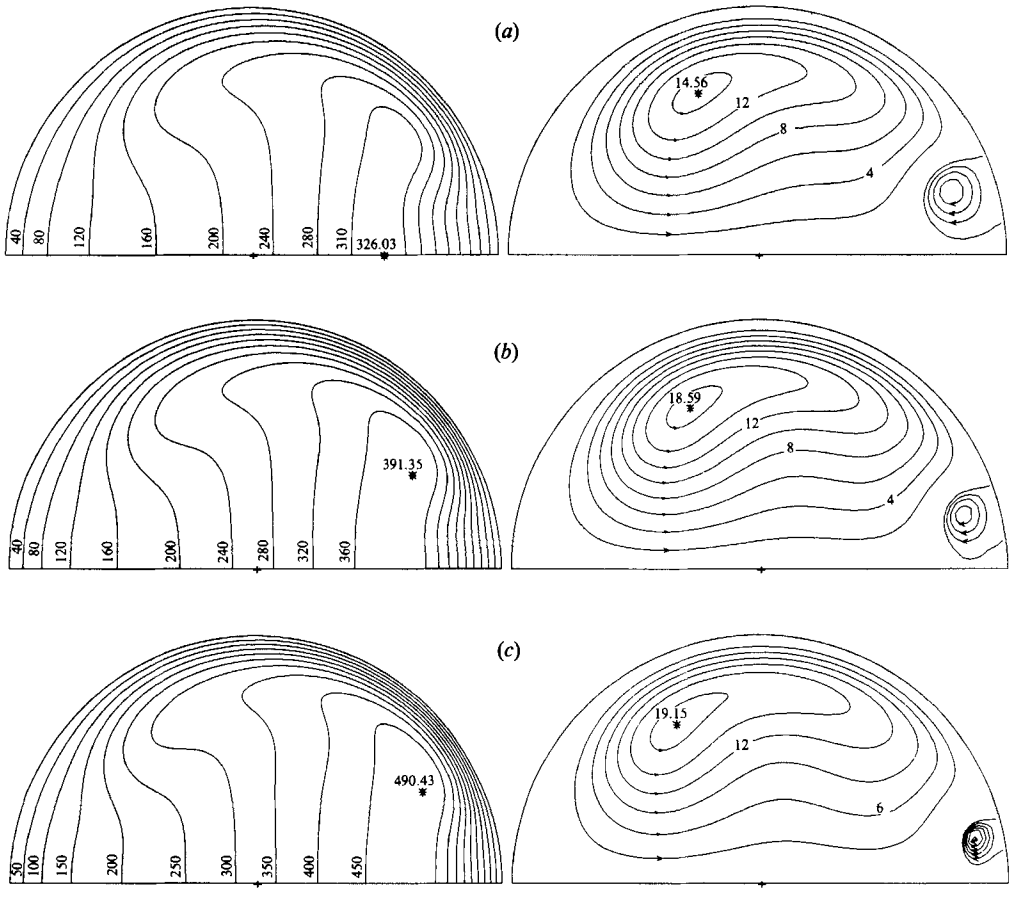

FIGURE 7. Axial velocity contours and secondary flow streamlines for doubly unstable branch of second solution family. (*a*) $D = 3100$; (*b*) 4000; (*c*) 5500.

friction-factor ratio γ_s/γ_c, where the subscripts s and c denote a straight and a curved tube respectively, of the same cross-section and carrying the same flux. Figure 8 compares values of this quantity calculated from our results with values reported in previous studies. Agreement among the different results is very good, with the exception, frequently noted previously (e.g. Dennis 1980), of the values calculated by Van Dyke (1978). The results of Soh & Berger (1987) reproduced in figure 8 are for curvature $\delta = 0.01$. A notable feature of the plot is that very similar values of the friction-factor ratio are seen for the various branches coexisting at any given value of D. Furthermore, the two stable solution branches seem to meet at the critical value $D \doteq 956$ at which the four-vortex solution ceases to exist; the same is true for the new family (two unstable branches), which seems to join the primary branch at $D \doteq 2494$. These observations are, however, misleading, and indicate that the friction-factor ratio is an inappropriate parameter for differentiating among different solution branches.

A more useful approach is to use as the state function the value of one of the velocity components at a particular point in the computational domain. Figure 9 shows, for the physically meaningful range of $D (< 6000)$, a bifurcation diagram based on the radial velocity at $r = 0.9$, $\alpha = 0$, together with the secondary flow

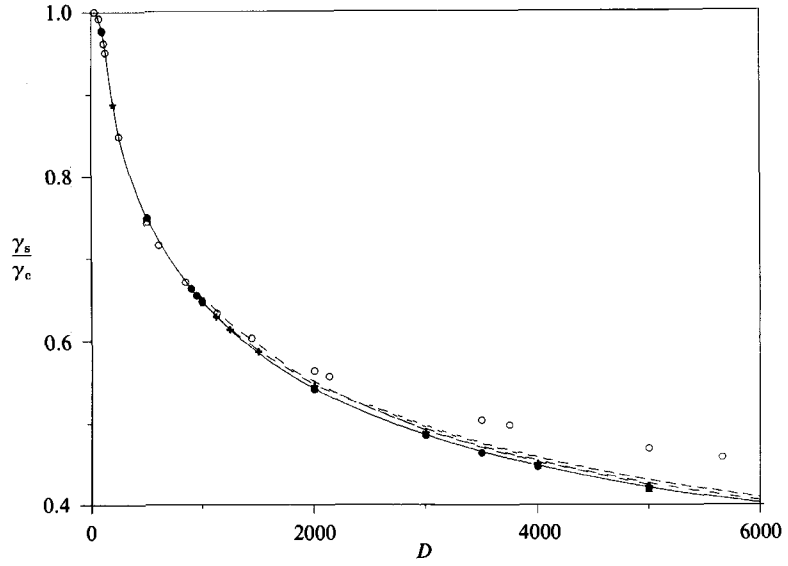

FIGURE 8. Comparison of friction-factor ratios. ——, Primary solution branch; ——, four-vortex solutions (first solution family); —·—, new solution family. ●, +. Dennis & Ng (1982) two- and four-vortex solutions respectively; ●, Soh & Berger (1987) two-vortex solution ($\delta = 0.01$); ○, Van Dyke (1978); X, ▲, Yang & Keller (1986*a*) stable two- and four-vortex solutions respectively.

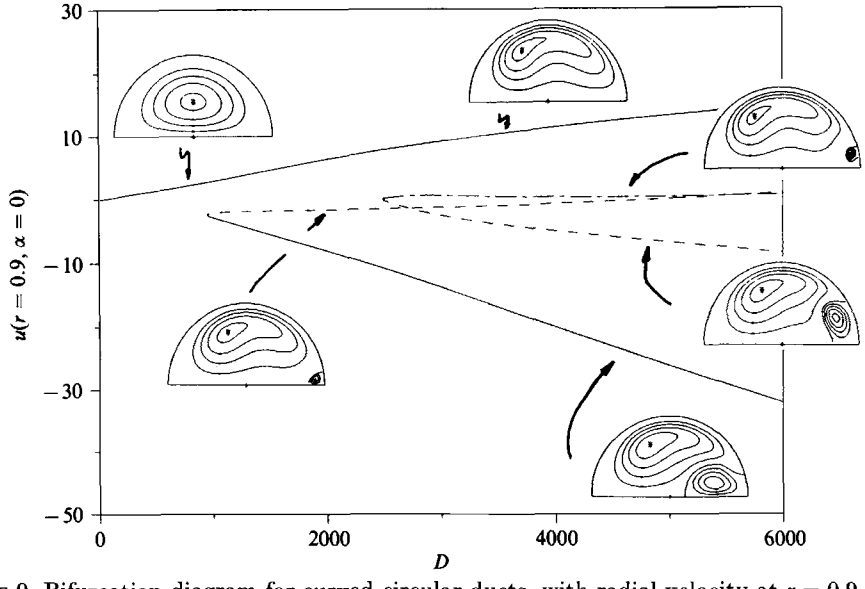

FIGURE 9. Bifurcation diagram for curved circular ducts, with radial velocity at $r = 0.9$ on plane of symmetry as state variable. Secondary flow streamlines are shown on each branch. ——, Stable solution; ——, unstable solution; —·—, doubly unstable solution.

streamlines representative of the different branches. The different nature of the four-vortex families can be easily distinguished, and the figure displays the qualitative features of bifurcation diagrams presented by Benjamin (1978). It also reproduces and complements some of the qualitative features of the bifurcation diagrams of Yang & Keller (1986*a*), but since they reported their results in terms of the friction-factor ratio, a more detailed comparison is not possible.

Many important features of the bifurcation diagrams can (and were, by Yang & Keller 1986*a*, *b*) be found directly by continuation methods. These methods do not, however, provide an assurance that all possible solution branches have been found; in particular, one-sided bifurcations giving rise to branches not linked to the primary solution may be present, as is indeed the situation pictured in figure 9. In order to gain greater insight into possible bifurcation patterns, we examine the morphogenesis of the bifurcation structure using the results of Benjamin (1978), as discussed in §2.

4.2. *Morphogenesis of bifurcation structure*

The analysis begins with the perfect problem of pressure-driven viscous azimuthal flow in a curved slit of infinite extent perpendicular to the flow direction. The stability of this flow was first studied by Dean (1928*b*) in the narrow-slit limit and was later extended for finite-gap problems. Extensive reviews as well as the most important literature references can be found in Chandrasekhar (1961) and Drazin & Reid (1981).

Poiseuille-like flow is the unique, unconditionally stable solution for small D. As the value of Dean number increases, there exists a critical D where the Poiseuille flow profile bifurcates to a cellular structure such as that observed in Couette flow (Taylor 1923). The critical values of D and the natural wavelength of the cells have been dttermined by solving the perturbation equations for axisymmetric disturbances (see e.g. Reid 1958). Within the cellular structure, a pair of adjacent cells represents a rectangular 'duct', which provides the basis for our subsequent computations. The lateral duct boundaries, at which there is no slip at present, are along the line of symmetry where flow is inward, by analogy with the situation in curved ducts (figure 1). We solved the system equations for rectangular ducts of small curvature (Ward-Smith 1980) using orthogonal collocation with Chebyshev polynomials in both the radial and axial directions as basis functions. For symmetry reasons thc computational domain is that of one cell of the secondary flow.

The natural intermediate stage between the perfect problem and the situation of ultimate interest, a duct of circular cross-section, is a duct of square cross-section. We begin, however, with a rectangular duct of aspect ratio 1.592, which is that given by the stability analysis of the perfect problem as the natural wavelength of the cell at the bifurcation point. This problem has a simpler bifurcation structure than does that in a square duct, because of a transcritical bifurcation at an aspect ratio of 1.426, noted by Winters (1987). The bifurcation structure for the square duct is consequently easier to understand if the most important features of that for the duct of aspect ratio 1.592 is described first.

The linear stability analysis results (Dean 1928*b*; Drazin & Reid 1981) were reproduced by the numerical scheme, which was then used to extend the bifurcation diagram beyond the first bifurcation point. The picture that emerges, for the conceptual flow through a single 'duct' (without slip on the cell boundaries) of constant aspect ratio, is shown in figures 10 and 11; the radial velocity at a specific point on the cell axis of symmetry is used as the flow parameter, as in figure 9 for the circular ducts. The bifurcation from the (primary) Poiseuille flow to the cellular structure (stable two-vortex secondary flow) is at $D = 53.88$. Here the Poiseuille flow becomes unstable, remaining so until $D = 75.95$, where a second bifurcation gives rise to an unstable four-vortex solution pattern, followed by a third bifurcation to a six-vortex solution, at $D = 123.95$. At still higher D additional bifurcations are observed, with multiple vortices, but we have not attempted to characterize them further. As

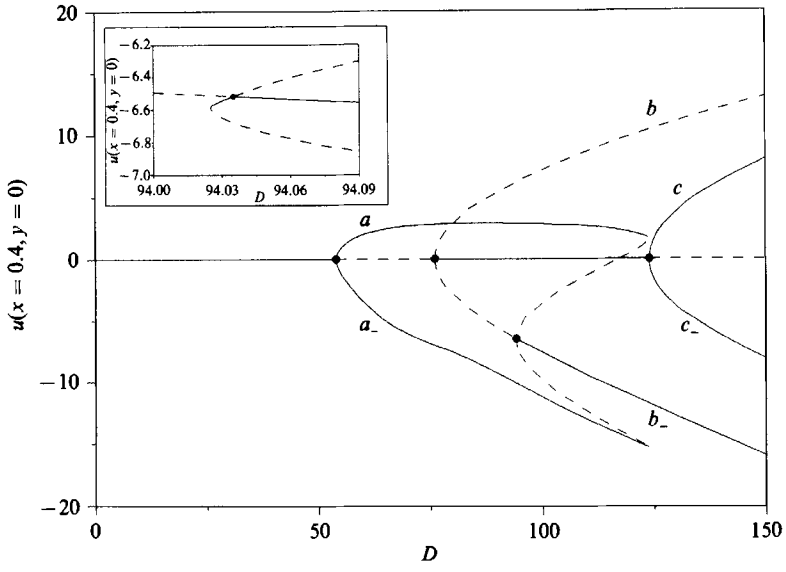

FIGURE 10. Bifurcation diagram for perfect problem for aspect ratio of 1.592. Region around $D = 94$ is expanded in inset. Solid and broken lines denote stable and unstable solutions respectively, and dots denote bifurcation points. Labels on branches refer to streamlines in figure 11; a minus sign subscript denotes phase shift.

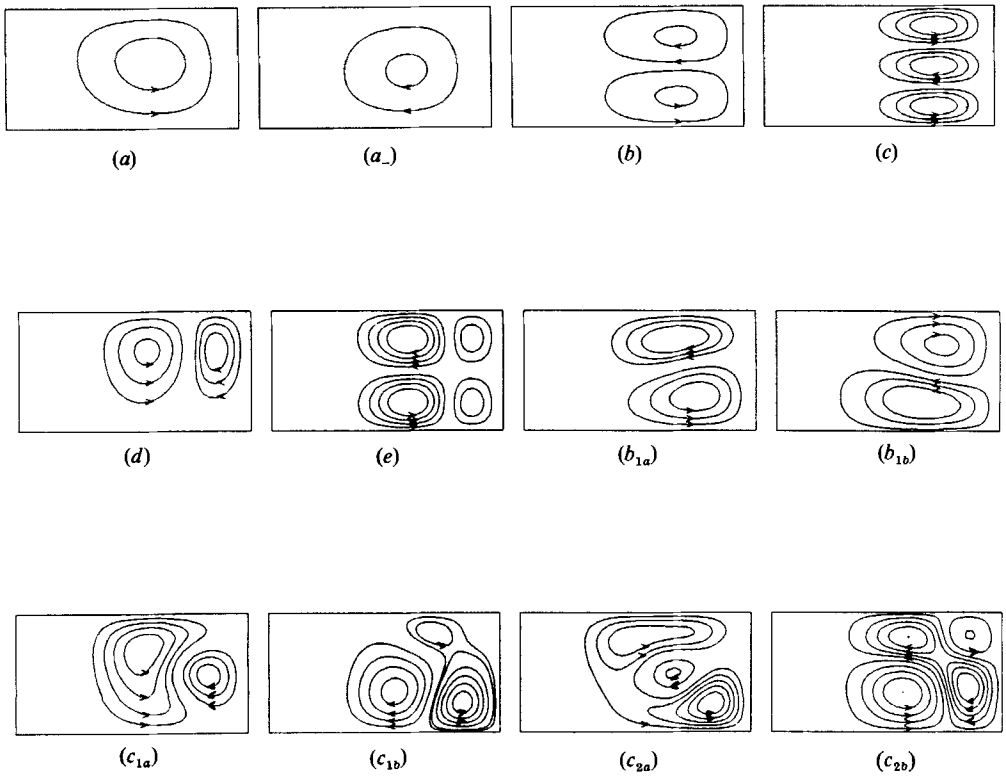

FIGURE 11. Secondary flow streamlines for branches labelled on perfect-problem bifurcation diagrams (figures 10, 13 and 14).

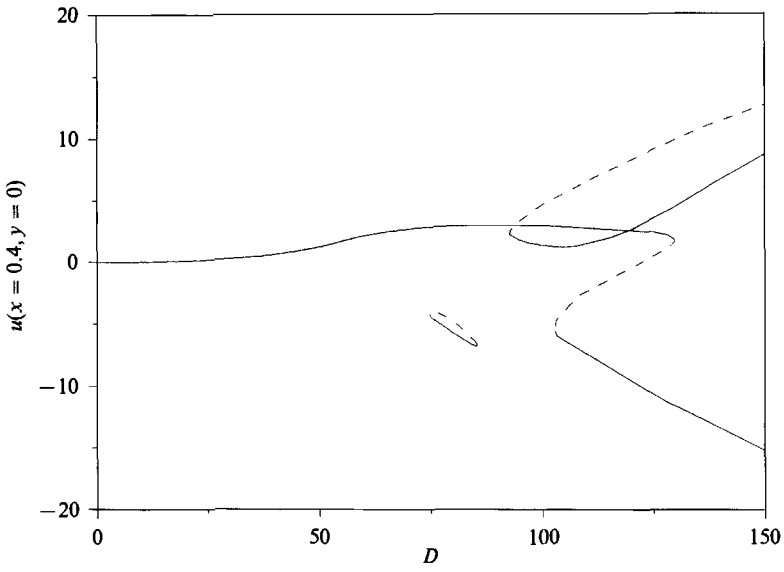

FIGURE 12. Bifurcation structure for rectangular duct with stickiness parameter = 0.1125. Smaller isola disappears with small increase in parameter, and larger one when parameter ≈ 0.31.

noted in §2, a half-period shift in the two-vortex solution leaves an equivalent flow structure, so that two branches emerge symmetrically from the first bifurcation point (Benjamin 1978); a quarter-period shift leads to the same conclusion for the second bifurcation point, and so on.

The branches emerging from the first bifurcation point give rise to a closed curve, with a pair of turning points at $D = 123.64$ beyond which the branches continue as unstable solutions with four vortices, but with much two-vortex character (the additional vortices are weak). The new vortices appear near the outer wall, grow and finally occupy half the domain at another bifurcation point at $D = 94.03$ (expanded in figure 10), where the closed two-vortex curve meets one four-vortex family arising from the bifurcation at $D = 75.95$. The latter then continues as a stable four-vortex solution. The other four-vortex solution is unstable up to at least $D = 500$, while the six-vortex branches are both stable at least this far; however, as the subsequent discussion indicates, the unstable four-vortex branch seems to meet one of the six-vortex branches at some point. Note that because of the choice of state variable in figure 10, crossing of branches in the figure does not necessarily imply a bifurcation point; bifurcation points are labelled explicitly.

Next, with the aspect ratio fixed, the boundary conditions along the lateral walls were changed by adding 'stickiness'; this was done by introducing a parameter that, in going continuously from 0 to 1, changed the boundary conditions from slip to no slip. The introduction of stickiness breaks the symmetry of the perfect problem, as described by Benjamin (1978); figure 12 shows the decoupled solutions when the parameter describing stickiness has the value 0.1125. There are now at least three distinct solution families. The primary solution at low D now is the one having a two-vortex secondary flow pattern; it develops from the Poiseuille flow and from the upper part of the two-vortex solution curve of the perfect problem, without the existence of any bifurcation points. The stable four-vortex and the intervening unstable solution at larger D are also part of this family. The second solution family

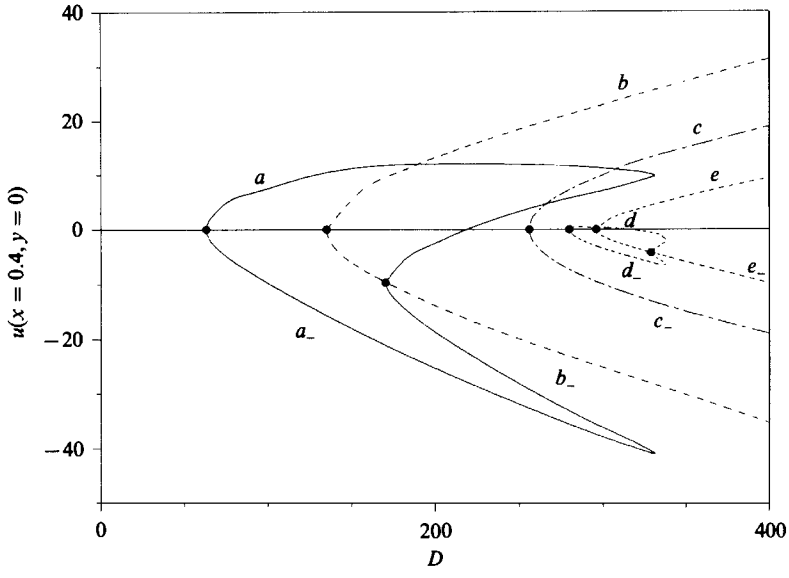

FIGURE 13. Primary bifurcation diagram for perfect problem for square duct, showing only branches arising from the primary solution. Different line types are for clarity, and do not reflect stability characteristics. Labels on branches labels refer to streamlines in figure 11; a minus-sign subscript denotes phase shift.

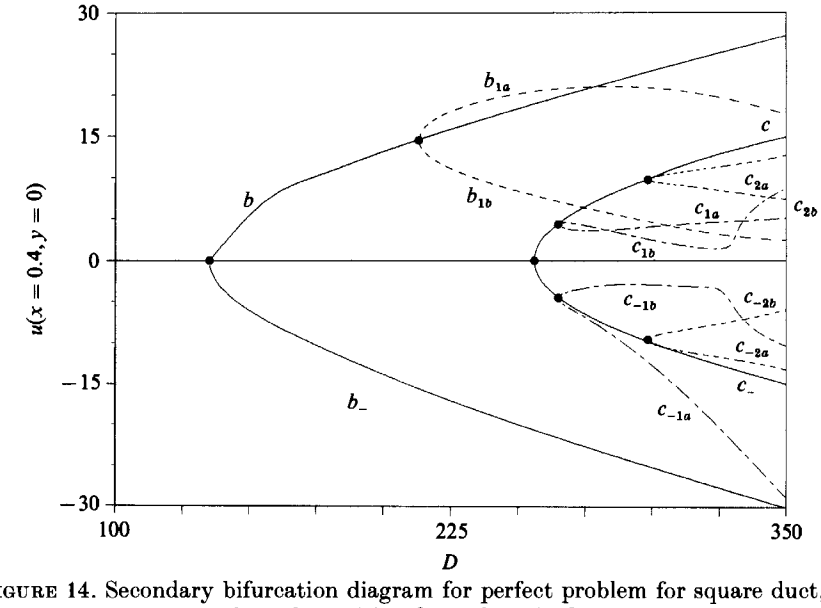

FIGURE 14. Secondary bifurcation diagram for perfect problem for square duct, showing branches arising from those in figure 13.

is an isola representing the lower branch of the two-vortex solution and the unstable part of the lower four-vortex solution of the perfect problem. The third family is also an isola, arising in similar fashion from the unstable four-vortex and one of the six-vortex branches, an observation which prompted the remark in the previous paragraph regarding the likelihood that these two branches meet even in the perfect problem. The primary branch is relatively insensitive to changes in the parameter

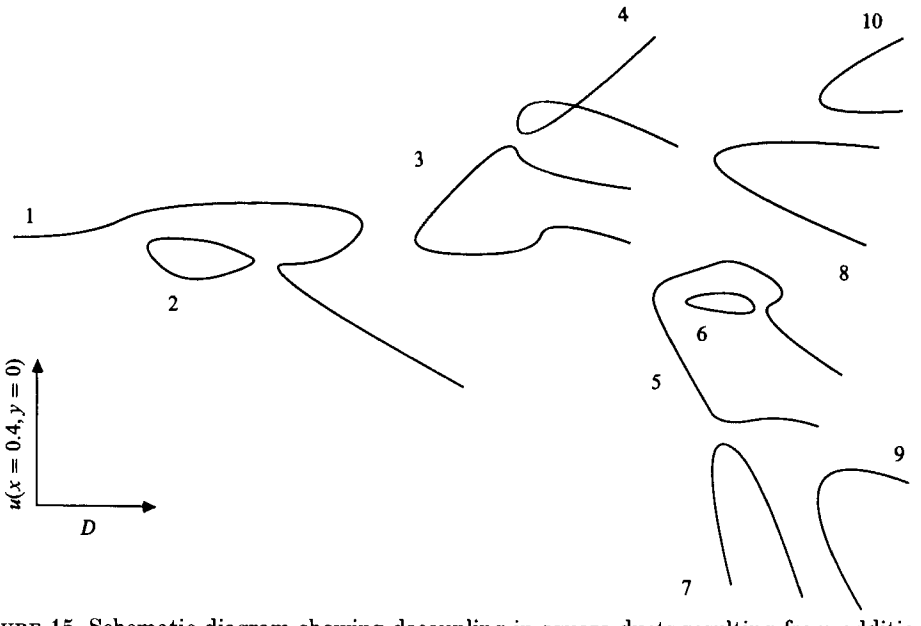

FIGURE 15. Schematic diagram showing decoupling in square ducts resulting from addition of stickiness.

describing stickiness, but the isolae shrink as the stickiness increases and disappear before the no-slip limit is reached. The first isola vanishes when the stickiness parameter exceeds by a small amount that used in preparing figure 12, while the second persists to beyond 0.31.

Our conjecture is that isola formation by branches differing by one pair in vortex number continues at higher vortex numbers, and that most of these isolae vanish by the time the no-slip limit is reached. Thus, in the no-slip limit (curved duct, aspect ratio 1.592, with solid walls) there appears to exist only one solution family, exhibiting two-vortex character up to a turning point where it becomes unstable and develops mixed two- and four-vortex character. After another turning point the solution is stable again, and this four-vortex branch exists up to the upper limit of the parameter range (laminar flow region). This result is qualitatively consistent with the most important features previously observed in experimental and theoretical studies of flow in rectangular ducts, e.g. Cheng & Akiyama (1970), Joseph *et al.* (1975), De Vriend (1981), Shanthini & Nandakumar (1986) and Winters (1987).

For square ducts the morphogenesis of the bifurcation structure was also examined with the perfect problem as the starting point, but now with the constraint of unit aspect ratio imposed for the formation of secondary flow cells. The bifurcation structure is much more complex than that for an aspect ratio of 1.592, the major qualitative differences being the existence, at relatively low D, of secondary bifurcation points, i.e. on the solution branches exhibiting cellular secondary flow structure. Hence, in addition to the two-, four- and six-vortex solution families developing from the Poiseuille solution, solutions exhibiting 2+2 and 4+4 vortex structure are seen. Additional multiple-vortex solutions also arise from the Poiseuille flow beyond the six-vortex bifurcation point. The results are summarized in figures 13 and 14, showing the bifurcations from the primary Poiseuille solution and the secondary bifurcations respectively; corresponding secondary flow streamlines are shown in figure 11.

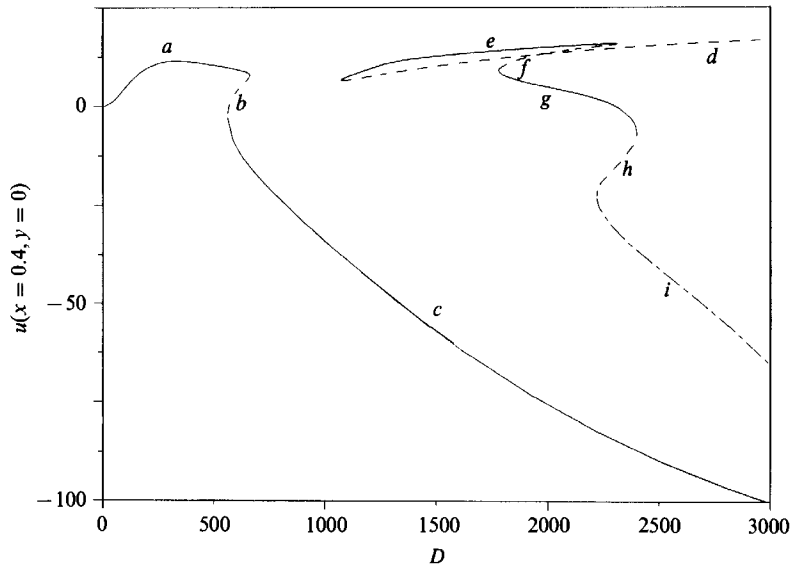

FIGURE 16. Bifurcation diagram for flow in square curved ducts: ——, stable solution; — —, unstable solution; —·—, doubly unstable solution. Labels on branches refer to figure 17.

The introduction of stickiness decouples the solutions, as shown qualitatively (for clarity) in figure 15, with the different solution branches displaying different forms of behaviour as stickiness is increased. Branches 2, 4, 5, 6 and 8 form isolae and then vanish before the no-slip limit is reached, while branches 7, 9 and 10 move rapidly to regions of high Dean number (> 5000). The only solutions remaining in the Dean-number range of usual interest are shown in figures 16 and 17, which include a new family in addition to that obtained for an aspect ratio of 1.592; this is a consequence of the transcritical bifurcation at an aspect ratio of 1.426, reported by Winters (1987). The new family consists of stable, unstable and doubly unstable (two positive eigenvalues) branches, which arise from the secondary bifurcations in the perfect problem. The family comprises a stable two-vortex solution linked through a turning point at either end to additional solutions. At one end the link is to an unstable four-vortex solution, and at the other to a series of folds, on which most of the solutions are characterized by multiple vortices. As figure 17 shows, the streamlines of these solutions are quite different from those in the first family, even when the number of secondary flow vortices is the same.

The qualitative and quantitative agreement with the calculations of Winters (1987) is very good. Winters reports results only up to $D \sim 2000$ and hence does not include the entire structure of the isolated solution family, but as shown in table 1 the turning points common to his work (for curvature 0.02) and ours are within about 5% of each other. Since Winters does not show the axial velocity profiles or secondary flow streamlines for the second family of solutions, a comparison with the corresponding streamlines shown in figure 17 is not possible. An additional aspect is that Winters considers asymmetric solutions, and finds the second family to be joined to the first by an asymmetric solution branch, which is obviously absent in our system. He also finds the four-vortex solution on the first family to be unstable to asymmetric disturbances.

What now remains is to go from a square geometry to a circular one. For this a curvilinear orthogonal coordinate system was used that is characterized by a

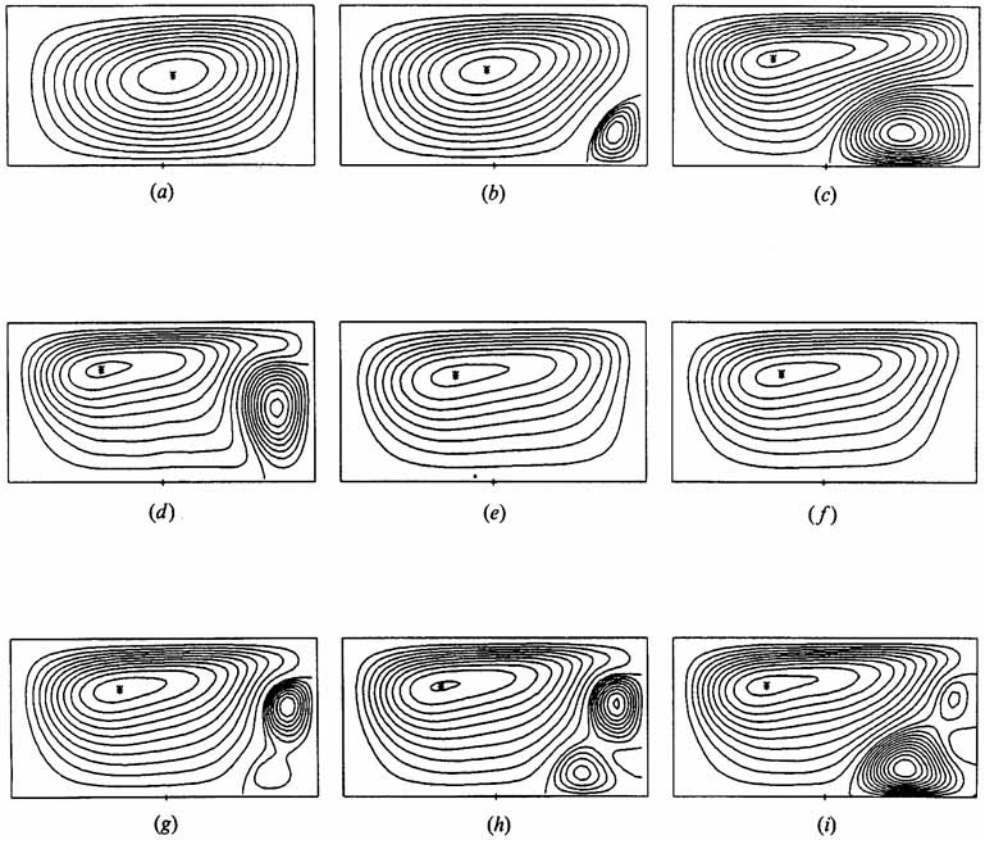

FIGURE 17. Secondary flow streamlines for flow in a curved duct of square cross-section, for branches labelled in figure 16. Values of D: (*a*) 450; (*b*) 642; (*c*) 2215; (*d*) 2900; (*e*) 1763; (*f*) 1953; (*g*) 1918; (*h*) 2386; (*i*) 2810.

Branches	D (this work)	D (Winters 1987)
ab	662.132	683.26
bc	562.097	579.25
de	1073.090	1112.83
ef	2314.055	
fg	1779.824	
gh	2396.406	
hi	2217.626	

TABLE 1. Turning points for square ducts. Branch labels refer to figure 17.

parameter, β, giving rise to different cross-sections with circular and square geometries as the two limits. The system equations were written in terms of the coordinates

$$\tilde{r} = (x^2 + y^2 - \beta x^2 y^2)^{\frac{1}{2}} \tag{23}$$

and

$$\tilde{\alpha} = \arctan\left(\frac{y}{x} e^{\beta(x^2-y^2)/2}\right) \tag{24}$$

and solved using an expansion similar to that of (12) and (13). Continuation in the shape parameter allows a smooth transition between the square and circular tube limits, but the nature of the coordinate system slows convergence significantly and also requires an expansion of high order for geometries near the rectangular limit. The continuation steps therefore have to be very small near the limit of a computational domain with sharp corners. The result of the transformation is seen in a comparison of figures 16 and 9, which are structurally similar. However, the new solution family is much simpler in circular ducts than in square ducts, and neither of the two solutions is stable even to symmetric disturbances. A notable trend is that the turning point between the primary two-vortex and the unstable solution rapidly moves to higher D as the cross-section approaches circularity, which makes it difficult to detect by continuation on the primary solution branch. The other two turning points remaining move to higher D much more slowly as the geometry approaches circularity.

5. Concluding remarks

While the bifurcation structures of flows in curved ducts of various cross-sections have become clearer in recent years, several issues have remained unresolved, particularly for ducts of circular cross-section. The results presented here appear to resolve some of these issues for ducts of small curvature. In particular, the stability to symmetric disturbances has been characterized and an additional family of solutions has been identified. Perhaps more important is that Benjamin's (1978) well-known results have been shown to be useful not just for coordinate transformations (e.g. Nandakumar & Masliyah 1982), but particularly for the utility of the perfect problem as a link between solution families that are not linked in a real, imperfect situation. Unresolved issues include the possibility of asymmetric solutions and the response to asymmetric disturbances, and the effects of curvature.

We are indebted to A. N. Beris for his frequent assistance and advice, and for his comments on this manuscript, and to R. A. Brown for useful discussions. The support of the National Science Foundation under grant CBT-8746050, including access to the Pittsburgh Supercomputing Center, is gratefully acknowledged.

REFERENCES

BARUA, S. N. 1963 On secondary flow in stationary curved pipes. *Q. J. Mech. Appl. Maths* **16**, 61–77.

BENJAMIN, T. B. 1978 Bifurcation phenomena in steady flows of a viscous fluid. I. Theory. *Proc. R. Soc. Lond.* A **359**, 1–26.

BERGER, S. A., TALBOT, L. & YAO, L.-S. 1983 Flow in curved pipes. *Ann. Rev. Fluid Mech.* **15**, 461–512.

CHANDRASEKHAR, S. 1961 *Hydrodynamic and Hydromagnetic Stability*, Chapter 8. Oxford University Press.

CHENG, K. C. & AKIYAMA, M. 1970 Laminar forced convection heat transfer in curved rectangular channels. *Intl J. Heat Mass Trans.* **13**, 471–490.

CHENG, K. C., INABA, T. & AKIYAMA, M. 1985 Flow visualization studies of secondary flow patterns and centrifugal instability in curved circular and semicircular pipes. In *Flow Visualization III* (ed. W. J. Yang), *Third Intl Symp. on Flow Visualization, 1983, Ann Arbor, Michigan*, pp. 531–536. Springer.

CHENG, K. C., NAKAYAMA, J. & AKIYAMA, M. 1979 Effect of finite and infinite aspect ratios on flow patterns in curved rectangular channels. In *Flow Visualization* (ed. T. Asanuma), *Intl Symp. on Flow Visualization, 1977, Tokyo, Japan*, pp. 181–186. Hemisphere.

COLLINS, W. M. & DENNIS, S. C. R. 1975 The steady motion of a viscous fluid in a curved tube. *Q. J. Mech. Appl. Maths* **28**, 133–156.

DEAN, W. R. 1927 Note on the motion of fluid in a curved pipe. *Phil. Mag.* **4**, (7) 208–223.

DEAN, W. R. 1928*a* The streamline motion of fluid in a curved pipe (second paper). *Phil. Mag.* **5**, (7) 673–695.

DEAN, W. R. 1928*b* Fluid motion in a curved channel. *Proc. R. Soc. Lond.* A **121**, 402–420.

DENNIS, S. C. R. 1980 Calculation of the steady flow through a curved tube using a new finite-difference method. *J. Fluid Mech.* **99**, 449–467.

DENNIS, S. C. R. & NG, M. 1982 Dual solutions for steady laminar flow through a curved tube. *Q. J. Mech. Appl. Maths* **35**, 305–324.

DE VRIEND, H. J. 1981 Velocity redistribution in curved rectangular channels. *J. Fluid Mech.* **107**, 423–439.

DRAZIN, P. G. & REID, W. H. 1981 *Hydrodynamic Stability*, Chapter 3. Cambridge University Press.

GOTTLIEB, D. & ORSZAG, S. A. 1977 *Numerical Analysis of Spectral Methods: Theory and Applications*. SIAM.

ITŌ, H. 1987 Flow in curved pipes. *Japan. Soc. Mech. Engrs Intl J.* **30**, 543–552.

JOSEPH, B., SMITH, E. P. & ADLER, R. J. 1975 Numerical treatment of laminar flow in helically coiled tubes of square cross section. *AIChE J.* **21**, 965–974.

KELLER, H. B. 1977 Numerical solution of bifurcation and nonlinear eigenvalue problems. In *Applications of Bifurcation Theory* (ed. P. H. Rabinowitz), pp. 359–384. Academic.

KELLER, H. B. 1982 Continuation methods in computational fluid dynamics. In *Numerical Methods and Physical Aspects of Aerodynamic Flows* (ed. T. Cebeci), pp. 3–13. Springer.

KUBÍČEK, M. & MAREK, M. 1983 *Computational Methods in Bifurcation Theory and Dissipative Structures*. Springer.

LANCZOS, C. 1956 *Applied Analysis*, Chapter 7. Prentice-Hall.

MASLIYAH, J. H. 1980 On laminar flow in curved semicircular ducts. *J. Fluid Mech.* **99**, 469–479.

MCCONALOGUE, D. J. & SRIVASTAVA, R. S. 1968 Motion of a fluid in a curved tube. *Proc. R. Soc. Lond.* A **307**, 37–53.

NANDAKUMAR, K. & MASLIYAH, J. H. 1982 Bifurcation in steady laminar flow through curved tubes. *J. Fluid Mech.* **119**, 475–490.

NANDAKUMAR, K., MASLIYAH, J. H. & LAW, H.-S. 1985 Bifurcation in steady laminar mixed convection flow in horizontal ducts. *J. Fluid Mech.* **152**, 145–161.

REID, W. H. 1958 On the stability of viscous flow in a curved channel. *Proc. R. Soc. Lond.* A **244**, 186–198.

SHANTHINI, W. & NANDAKUMAR, K. 1986 Bifurcation phenomena of generalized newtonian fluids in curved rectangular ducts. *J. Non-Newtonian Fluid Mech.* **22**, 35–60.

SOH, W. Y. 1988 Developing fluid flow in a curved duct of square cross-section and its fully developed dual solutions. *J. Fluid Mech.* **188**, 337–361.

SOH, W. Y. & BERGER, S. A. 1987 Fully developed flow in a curved pipe of arbitrary curvature ratio. *Intl J. Numer. Meth. Fluids* **7**, 733–755.

TAYLOR, G. I. 1923 Stability of a viscous liquid contained between two rotating cylinders. *Phil. Trans. R. Soc. Lond.* A **223**, 289–343.

VAN DYKE, M. 1978 Extended Stokes series: laminar flow through a loosely coiled pipe. *J. Fluid Mech.* **86**, 129–145.

WARD-SMITH, A. J. 1980 *Internal Fluid Flow*, Chapter E. Clarendon.

WINTERS, K. H. 1987 A bifurcation study of laminar flow in a curved tube of rectangular cross-section. *J. Fluid Mech.* **180**, 343–369.

WINTERS, K. H. & BRINDLEY, R. C. G. 1984 Multiple solutions for laminar flow in helically-coiled tubes. *AERE Rep.* 11373, AERE Harwell, UK.

YANG, Z.-H. & KELLER, H. B. 1986*a* Multiple laminar flows through curved pipes. *Appl. Num. Maths* **2**, 257–271.

YANG, Z.-H., KELLER, H. B. 1986*b* Multiple laminar flows through curved pipes. In *Proc. Tenth Intl Conf. on Numerical Methods in Fluid Dynamics, Beijing 1986* (ed. F. G. Zhuang, Y. L. Zhu), pp. 672–676. Springer.